Photochemistry and Photobiology, 2019, 95: 1195–1204

Conformational Dynamics of Sensory Rhodopsin II in Nanolipoprotein and Styrene–Maleic Acid Lipid Particles

Wageiha Mosslehy[1], Natalia Voskoboynikova[1], Alexandr Colbasevici[1], Adrian Ricke[1], Daniel Klose[1,2], Johann P. Klare[1], Armen Y. Mulkidjanian[1,3] and Heinz-Jürgen Steinhoff*[1]

[1]Department of Physics, University of Osnabrück, Osnabrück, Germany
[2]Laboratory of Physical Chemistry, ETH Zürich, Zürich, Switzerland
[3]School of Bioengineering and Bioinformatics, Lomonosov Moscow State University, Moscow, Russia

Received 5 December 2018, accepted 3 March 2019, DOI: 10.1111/php.13096

ABSTRACT

Styrene–maleic acid lipid particles (SMALPs) provide stable water-soluble nanocontainers for lipid-encased membrane proteins. Possible effects of the SMA-stabilized lipid environment on the interaction dynamics between functionally coupled membrane proteins remain to be elucidated. The photoreceptor sensory rhodopsin II, *Np*SRII and its cognate transducer, *Np*HtrII, of *Natronomonas pharaonis* form a transmembrane complex, $NpSRII_2/NpHtrII_2$ that plays a key role in negative phototaxis and provides a unique model system to study the light-induced transfer of a conformational signal between two integral membrane proteins. Photon absorption induces transient structural changes in *Np*SRII comprising an outward movement of helix F that cause further conformational alterations in *Np*HtrII. We applied site-directed spin labeling and time-resolved optical and EPR spectroscopy to compare the conformational dynamics of $NpSRII_2/NpHtrII_2$ reconstituted in SMALPs with that of nanolipoprotein particle and liposome preparations. *Np*SRII and $NpSRII_2/NpHtrII_2$ show similar photocycles in liposomes and nanolipoprotein particles. An accelerated decay of the M photointermediate found for SMALPs can be explained by a high local proton concentration provided by the carboxylic groups of the SMA polymer. Light-induced large-scale conformational changes of $NpSRII_2/NpHtrII_2$ observed in liposomes and nanolipoprotein particles are affected in SMALPs, indicating restrictions of the protein's conformational freedom.

INTRODUCTION

The preparation of homogeneous and functional samples for the spectroscopic investigation of membrane protein structure and dynamics, especially for nuclear magnetic resonance (NMR) (1), electron paramagnetic resonance (EPR) (2) and cryo-electron microscopy (3) is challenging. Delivery of single membrane proteins or membrane protein complexes in a native-like environment is also required for X-ray free electron lasers (X-FEL), which may allow determination of the structure of single protein molecules in the near future (4). The most common method for membrane protein purification for the above-mentioned applications necessitates extraction from the biological membrane into detergent micelles, which could negatively affect the stability and activity of purified proteins (5).

Currently, two membrane mimetic approaches, which provide monodisperse nanoparticles of ~ 10–15 nm diameter containing membrane proteins, are under development. In these approaches a protein-lipid core is surrounded and stabilized either by an amphipathic protein belt, in the so-called nanodiscs or nanolipoprotein particles (NLPs), (6–8) or by a styrene–maleic acid (SMA) copolymer, yielding SMA-lipid particles (SMALPs) (9,10). Both NLPs and SMALPs can be prepared from a variety of lipid mixtures and even native lipids of membrane extracts. It was reported that such preparations are well suitable for single molecule experiments or EPR spectroscopy (11–14). For EPR-based intramolecular distances measurements using double electron–electron resonance (DEER) (15) the reconstitution of the spin-labeled proteins into NLPs or SMALPs is highly advantageous because the dipolar coupling between spin labels of different proteins in the pseudo-two-dimensional environment of proteoliposomes determines the intermolecular background. The contribution of this background can dominate the DEER signal imposing severe limits on sensitivity, distance range and data interpretation (16,17). Although nowadays almost routinely used, a major drawback of the NLP methodology is that the proteins first have to be extracted from the native membrane using detergents, which subsequently must be removed completely for the assembly of the NLPs. Contrarily, the assembly of SMALPs does not require the use of detergents in any of its preparation steps. This advantage led to the most striking feature of SMALP systems, which is the possibility to extract membrane proteins directly from the native cell membranes, without any intermediate step, where the protein's immediate environment could be affected. Numerous studies have shown that this method can be successfully used to purify different membrane proteins (11,18–21) and membrane protein complexes, (13,22–25) and the molecular and functional properties of these nanoparticles have been studied in some detail (11,26,27). In general, the stability and activity of the proteins investigated in SMALPs were shown to be either similar to those in detergent micelles or improved, suggesting that the SMA-lipid particles can provide more native conditions (18,20,21,23). However, little is known about the possible influence of the SMA-stabilized lipid environment on large-scale conformational transitions, which may accompany or even only facilitate the function of a membrane protein or membrane

*Corresponding author email: hsteinho@uos.de (Heinz-Jürgen Steinhoff)

protein complex. In the present paper, we address this question by applying the SMALP approach to a membrane protein from the microbial rhodopsin family in the presence and absence of its cognate transducer protein and compare our results with those obtained with the protein(s) reconstituted into NLPs or liposomes.

The sensory rhodopsin II of *Natronomonas pharaonis* (*Np*SRII) is a membrane-embedded photoreceptor that mediates the photorepellent response to potentially harmful blue light. The protein performs its function in a complex with the receptor-specific transducer protein *Np*HtrII. *Np*SRII's structure and function are related to those of the light-driven proton pump bacteriorhodopsin (BR). Both rhodopsins contain an *all-trans*-retinal chromophore covalently bound to the seven helical (A-G) membrane protein via a protonated Schiff base (28,29). Photoexcitation of the retinal chromophore induces a photoreaction cycle, the so-called photocycle. The first reaction in this photocycle is the photochemical isomerization of the retinal from the *all-trans* to the 13-*cis* form, in association with the generation of intermediate K. Proton migration from the Schiff base to Asp75 leads to the L-to-M transition, coinciding with the proton release at the extracellular side if the sensor is not complexed with its cognate transducer, *Np*HtrII. During the long-lived M-state, helix F moves outward and induces a downstream conformational change in the tightly coupled transmembrane helix TM2 of *Np*HtrII, which, in turn, transmits the signal further to the intracellular two-component pathway, which modulates the swimming behavior of the cell (30–33). Decay of the intermediate M and generation of intermediates N and O in equilibrium with each other coincides with reprotonation of the deprotonated 13-*cis* Schiff base. The formation of the O-state is attributable to the retinal reisomerization from 13-*cis* to *all-trans*. Finally, the O-state decays back to the initial state of *Np*SRII.

In our previous paper, we reported the assembly of *Np*SRII/*Np*HtrII in SMALPs and showed that the *Np*SRII/*Np*HtrII complex retained its structural integrity as a native-like 2:2 dimer with the distance between spin labels bound at position 159 of *Np*SRII corresponding to the "V"-shaped conformation found in the crystal structure (25,34). Resonance Raman spectroscopy data confirmed that *Np*SRII reconstituted in SMALPs preserved the light-sensitive *all-trans* configuration of its retinal chromophore (25).

In this work, we compare the light-induced conformational dynamics of *Np*SRII, in the presence and absence of *Np*HtrII, reconstituted into SMALPs, NLPs and liposomes, using a set of time-resolved optical and EPR methods.

MATERIALS AND METHODS

Protein expression and purification. For purification purposes, all proteins had a C-terminal 6xHis-tag. *Np*SRII-His and *Np*HtrII$_{157}$-His (transducer construct truncated at position 157) and their respective cysteine mutants (*Np*SRII-L159C and *Np*HtrII$_{157}$-A94C) were expressed in *E. coli* BL21 (DE3) and purified according to Ref. (35–37) with minor modifications. Briefly, cells were grown in LB medium (with 50 mg mL^{-1} kanamycin; 37°C) to an optical density OD$_{578}$ of 0.8–1.0, and overexpression was induced by 0.5 mM IPTG. After induction, the cells were incubated for 3 h at 37°C. Afterward, the cells were harvested by centrifugation (15 min; 4200 ***g***; 4°C), washed, resuspended in cell washing buffer (25 mM NaP$_i$ pH 8.0; 150 mM NaCl; 2 mM EDTA; 1/100 culture volume) and disrupted by sonication (Branson Sonifier II W-250). The membrane fraction was isolated by centrifugation (1.5 h; 50 000 ***g***; 4°C), and membrane proteins were solubilized overnight (4°C) in buffer A (50 mM NaP$_i$ pH 8.0; 300 mM NaCl; 2% [w/v] n-dodecyl-β-D-maltoside [DDM]). The solubilized membrane proteins were isolated by centrifugation (1.5 h; 50 000 ***g***; 4°C) and incubated (2 h) with Ni-NTA Superflow (Qiagen) material pre-equilibrated in buffer B (50 mM NaP$_i$ pH 8.0; 300 mM NaCl; 0.05% (w/v) DDM) containing 15 mM imidazole. Unspecific bound proteins were removed by washing with buffer B containing 30 mM imidazole. The His-tagged proteins were eluted with buffer B containing 200 mM imidazole. From the fractions containing the desired protein, imidazole was removed by dialysis against buffer C (10 mM Tris pH 8.0; 500 mM NaCl; 0.05% (w/v) DDM). If not used directly for spin labeling and reconstitution, protein solutions were stored at −80°C.

The scaffolding protein MSP1E3D1 used for NLP preparations was expressed in *E. coli* BL21 (DE3) cells and purified according to Ref. (38) with minor modifications. Briefly, transformed cells were grown in LB medium containing 50 mg mL^{-1} kanamycin at 37°C to an optical density OD$_{580}$ of 1.0. The overexpression of the protein was induced by addition of IPTG to a final concentration of 0.5 mM. After an induction period of 4 h at 37°C, cells were harvested (4200 ***g***; 15 min; 4°C) and resuspended (1/100 culture volume) in buffer D (300 mM NaCl, 40 mM Tris [pH 8.0]) containing 1% Triton X-100. Cells were disrupted by sonication (Branson Sonifier II W-250). The cell suspension was cleared by centrifugation (50 000 ***g***; 45 min; 4°C). The cleared supernatant was subsequently loaded onto Ni-NTA Superflow material pre-equilibrated with buffer D. The column was washed with four bed volumes of each of the following: (1) buffer D containing 1% Triton X-100; (2) buffer D containing 50 mM cholate; (3) buffer D; (4) buffer D containing 50 mM imidazole. MSP1E3D1 was eluted with buffer D containing 300 mM imidazole. Fractions containing MSP1E3D1 were pooled and dialyzed against 100 mM NaCl, 10 mM Tris (pH 8.0) buffer to remove imidazole. If not used directly for reconstitution, protein samples were flash frozen and stored at −80°C.

Spin labeling. The spin label (1-oxyl-2,2,5,5-tetramethylpyrroline-3-methyl) methanethiosulfonate (MTSSL; Enzo life sciences, NY) was covalently attached to the cysteine residues of both *Np*SRII-His and *Np*HtrII$_{157}$-His mutants solubilized in DDM as described previously (13). In brief, the purified protein was first reduced with 10 mM dithiothreitol (DTT) (12–16 h), which was then removed by dialyzing it against buffer C. Afterward, the protein was incubated 12–16 h with 1 mM MTSSL and excess label was removed by repeated dialysis. The resulting spin-labeled side chain is abbreviated as R1 in the following.

Preparation of proteoliposomes. Polar lipid extract of *Escherichia coli* membranes in chloroform was purchased from Avanti Polar Lipids, Inc. (Alabaster, AL). Lipids were transferred to a glass flask and the solvent was evaporated under a nitrogen flow. The resulting lipid film was dried under vacuum for at least 1 h, and then hydrated in buffer E (10 mM Tris pH 8.0; 150 mM NaCl) followed by 10 freeze-thaw cycles and. If not used directly, preparations were stored as aliquots at −80°C. Subsequently, before reconstitution, the lipid suspension was passed at least 11 times through a Mini-Extruder (Avanti Polar Lipids; Inc.) using polycarbonate membranes (Whatman) with a pore diameter of 400 nm.

The reconstitution of *Np*SRII or *Np*SRII/*Np*HtrII$_{157}$ into liposomes was performed by using SM-2 Bio-Beads (Bio-Rad Laboratories, München, Germany). Firstly, in case of reconstitution of *Np*SRII in complex with its cognate *Np*HtrII$_{157}$, solubilized *Np*SRII and *Np*HtrII$_{157}$ were mixed at a 1:1 molar ratio and incubated for 20 min on ice. Subsequently, the proteins were mixed with liposomes at a molar protein/lipid ratio of 1:172. For extracting DDM, the assembly mixture was incubated with extensively prewashed (methanol and water) Bio-Beads (1 g/4 mL) for 16 h at 4°C. After removal of Bio-Beads, the proteoliposomes were pelleted by centrifugation (15 min; 15 800 ***g***; 4°C), washed and then resuspended in buffer E to a final lipid concentration of 25 mM (20 mg mL^{-1}). Reconstitution in PML was performed according to Wegener *et al.* (30).

Preparation of SMA copolymer. Styrene–maleic acid (SMA) copolymer with a styrene to maleic acid molar ratio of 3:1 (MW 9500 Da; supplied as an aqueous sodium salt solution SMA 3000 HNa) was kindly provided as a gift by Cray Valley (Exton, PA). A 5% (w/v) solution of SMA, which was extensively dialyzed against buffer E, was used for the preparation of SMALPs.

Preparation of SMALPs. To form SMALP nanoparticles from proteoliposomes, the proteoliposome suspension (liposomes loaded with *Np*SRII or *Np*SRII/*Np*HtrII$_{157}$) was sonicated for 30 min in a bath sonicator (11). Then 1 mL of a 5% (w/v) solution of SMA copolymer

was added dropwise to 1 mL of the proteoliposome suspension to get a final lipid-to-SMA ratio of 1:2.5 (w/w). Afterward, the assembly mixture was allowed to equilibrate for 1 h at room temperature and then for 16 h at 4°C. The resulting samples were centrifuged (126 000 ***g***; 30 min; 4°C) to remove nonsoluble aggregates.

For direct reconstitution of *Np*SRII from *E. coli* membranes into SMALP nanoparticles, the membrane fraction of disrupted cells was isolated by centrifugation (50 000 ***g***, 1.5 h, 4°C). The pellet was resuspended in 1 mL buffer D, mixed at a ratio 1:1 (v/v) with a 5% (w/v) solution of SMA copolymer, and gently shaken at 4°C for 12 h. After centrifugation (50 000 ***g***, 1.5 h, 4°C), the supernatant was loaded onto a Ni-NTA column and the *Np*SRII filled SMALPs were washed and eluted with buffer D containing imidazole as described above.

Preparation of NLPs. NLPs were assembled *in vitro* according to Ref. (13) using MSP1E3D1 as a scaffold protein. The assembly was performed in buffer E (see: preparation of proteoliposomes) containing 5 mM DDM. For reconstitution of *Np*SRII or the *Np*SRII/*Np*HtrII$_{157}$ complex, polar lipid extract from *Escherichia coli* and MSP1E3D1 were added to the purified, DDM-solubilized *Np*SRII or *Np*SRII/*Np*HtrII$_{157}$. For the complex reconstitution, *Np*HtrII$_{157}$ was first mixed with *Np*SRII at a 1:1 molar ratio and then incubated for 20 min on ice before adding the lipids and MSP1E3D1. The final concentrations of the components were 0.76 mM lipids, 14 μM MSP1E3D1 and 7 μM *Np*SRII/*Np*HtrII$_{157}$. After incubation for 1 h at room temperature, the assembly mixture was incubated with SM-2 Bio-Beads overnight at 4 °C to remove DDM (50 mg of beads/mg of detergent). Bio-Beads were prewashed extensively with methanol and water. After removal of the Bio-Beads, nonsolubilized proteins and any aggregated materials were removed by centrifugation at 126 000 ***g*** for 15 min at 4°C. Samples were stored at 4°C until further use. Subsequently, preparations of NLPs were fractionated on a Superdex 200 10/200 GL column using an ÄKTA Purifier FPLC system, with a flow rate of 0.5 mL min^{-1} at 4°C.

Transient optical absorption spectroscopy. Transient optical absorption experiments were carried out as described in Ref. 39. A 50 W halogen lamp with an infrared cutoff filter (KG-2) and either 400, 430, 480, 500, 520, 550, 562, 575, 590 or 655 nm interference filters illuminated the sample-filled quartz cuvette inside a sample holder, which was temperature-controlled to 298 K. The transmitted light was passed through a monochromator and detected using a photodiode, while a flashlight with a flash duration of 80 μs equipped with a 475-nm edge filter provided excitation perpendicular to the transmission beam. The amplified signal was recorded with an analog-to-digital converter connected to a standard PC. For the transitions between the late photocycle intermediates ($t > 2$ ms) studied here, the kinetics determined by flashlight excitation were indistinguishable from those determined by pulsed laser excitation (40).

Continuous wave- and time-resolved EPR setup. Both continuous wave (cw) and time-resolved EPR measurements were performed as described previously (40). Room temperature cw EPR spectra were recorded on a home-built EPR spectrometer operating at ca. 9.5 GHz equipped with a dielectric resonator (Bruker Biospin, Germany). The microwave power was set to 1.0 mW, the B-field modulation amplitude was 0.35 mT or 0.15 mT in case of N*p*SRII-L159R1 and N*p*HtrII$_{157}$-A94R1, respectively. The sample temperature was stabilized by a gas stream through the resonator to 297 ± 1 K. A volume of 15 μL of sample at concentration of ~ 200 μM was loaded into a glass capillary (0.9 mm inner diameter). For time-resolved cw EPR measurements, samples were illuminated inside the resonator by a white LED (3 W power; Edixeon A; EDEW-3LA3-E3) through an infrared cutoff filter (KG-2) and a 500 nm edge filter for 1.5 s to allow for partial accumulation of activated *Np*SRII. The EPR transients were recorded for 4.5 s after illumination at fixed B-field positions using an analog-to-digital converter read out by a standard PC. The lock-in time constant was set to 100 ms, allowing to record the slow components of the relaxation of the *Np*SRII back to the initial state, for 35–100 B-field positions. Typically, 100–1000 time traces at each B-field position were averaged to achieve sufficient signal to noise ratio. The EPR difference spectra between the photo-activated and the initial states were recorded by detecting the EPR transients at different B-field values corresponding to a B-field scan. The cw EPR spectrum of the initial state was obtained concomitantly to the EPR transient traces by averaging the signal intensity detected during the 250 ms duration of the pretrigger before the illumination. The kinetics of the EPR signal changes were analyzed for selected B-field values where the difference spectra showed local extremes. For comparison to the optical transients, the EPR transients were fitted with tri-exponential functions.

RESULTS AND DISCUSSION

Several EPR studies (30,31,41) elucidated the light-induced conformational changes of *Np*SRII during the last years. The data obtained show that structural rearrangements occurring in the protein during the long-lived M-state of the *Np*SRII photocycle lead to an outward movement of helix F, which is analogous to the helix F motion observed for bacteriorhodopsin (BR) (42–44). Here, we follow these conformational transitions using EPR spectroscopy to study the possible influence of the encasement of the *Np*SRII/*Np*HtrII complex in NLPs and SMALPs. To monitor the light-induced conformational changes of *Np*SRII in the presence and absence of its transducer *Np*HtrII$_{157}$, the variant *Np*SRII-L159R1 with a nitroxide spin label bound at position 159 in helix F was selected (Fig. 1), which was shown to be highly sensitive to helix motion (30,31,41). A transient mobilization of the nitroxide side chain of L159R1 takes place during the photocycle due to the light-induced transient outward movement of helix F (see Fig. 1A), which can be detected using time-resolved EPR (30,31). *Np*SRII-L159R1 was reconstituted alone or in complex with *Np*HtrII$_{157}$ in three different lipid environments: liposomes, NLPs and SMALPs containing polar lipids from *Escherichia coli.*

Spin-label side-chain mobility

To analyze the effect of the different environments on the conformational dynamics of the receptor *Np*SRII, cw EPR spectra were recorded for *Np*SRII-L159R1 with and without the transducer *Np*HtrII$_{157}$ in liposomes, NLPs and SMALPs (Fig. 2A). The spectra of L159R1 are almost identical showing a powder-like spectral pattern with a resolved hyperfine line in the high field region. The presence of N*p*HtrII$_{157}$ does not significantly influence the behavior of L159R1 (25). This spectral shape indicates a strong sterical interaction between the nitroxide and neighboring residues of the protein as expected for the L159R1 side chain being buried between helices F and G (see Fig. 1A). Hence, the different lipid environments do not affect the nitroxide dynamics in the interior of *Np*SRII, indicating that the tertiary structure of the protein close to position 159 is not influenced.

The transducer variant *Np*HtrII$_{157}$-A94R1 in complex with *Np*SRII allows monitoring the dynamics of the coupled transducer close to the membrane-water interface. The spin label at this site has been shown to sensibly report on the conformation of the first HAMP domain of the transducer, which is engaged in an equilibrium between a more rigid, compact conformation and a more flexible, dynamic conformation (45). This site also has been used to trace the light-induced signal transfer from *Np*SRII to *Np*HrII (40). The cw EPR spectra of *Np*SRII/*Np*HtrII$_{157}$-A94R1 in liposomes, NLPs and SMALPs (Fig. 2B) exhibit a composite spectral shape, revealing the presence of at least two components related to mobile (vm, m) and immobile (i) fractions of the spin-label side chain. These components have been shown to reflect a conformational equilibrium of the HAMP domain (40). While the dynamics of the *Np*HtrII$_{157}$-A94R1 side chain with the protein reconstituted in NLPs is similar to that of the complex in liposomes, and consequently the equilibrium between

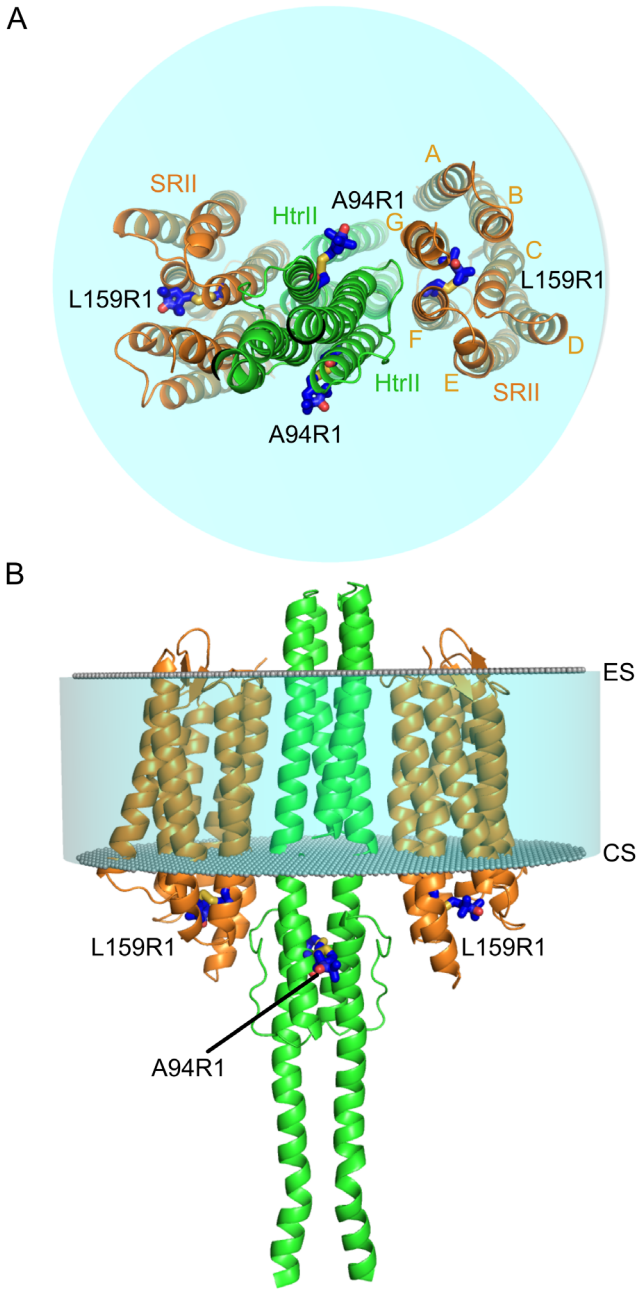

Figure 1. (A) View from the cytoplasm toward the extracellular space (labeled CS and ES in B, respectively) and (B) side view parallel to the membrane plane of the 2:2 complex of *Np*SRII and *Np*HtrII$_{157}$ (PDB: 1H2S(34)). The spin-labeled residues are depicted in blue.

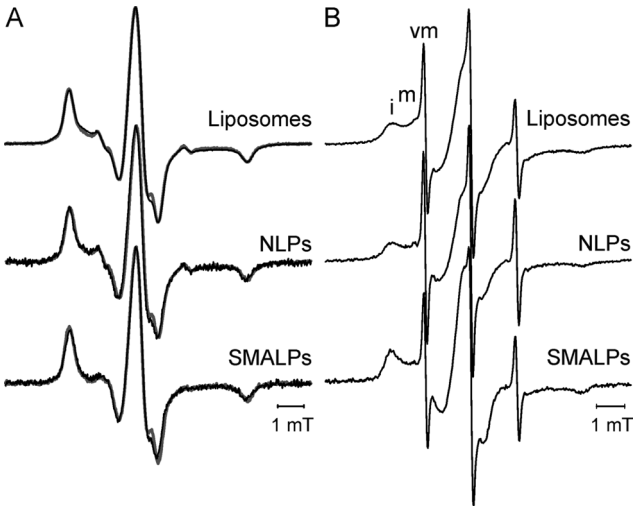

Figure 2. Room temperature cw EPR spectra of (A) *Np*SRII-L159R1 (black) compared to *Np*SRII-L159R1/*Np*HtrII$_{157}$ (25) (gray) and (B) *Np*SRII/N*p*HtrII$_{157}$-A94R1. The different mutants are reconstituted in liposomes, NLPs or SMALPs. All spectra are normalized to the maximum amplitude of the center line. The spectra for *Np*SRII/*Np*HtrII$_{157}$-A94R1 consists of at least two components, characterized by an immobilized (i) and a very mobile (vm) R1 side chain. A third, mobile component (m) is detectable by the spectral contribution visible between the two extremes.

the mobile and immobile components is not affected, the motion of the transducer R1 side chain in SMALPs is more restricted revealed by the more pronounced immobile component (i) and the equilibrium between the mobile and immobile components is shifted toward the immobile component. This finding indicates less flexibility of the protein in SMALPs.

The influence of the lipid environment on the photocycle kinetics

The light-induced reaction cycle, the so-called photocycle of *Np*SRII, triggers the signal transduction in the *Np*SRII$_2$/*Np*HtrII$_2$ complex (46). Lipid composition, temperature and pH may considerably influence the photocycle kinetics (5,46,47). Therefore, we performed flash-photolysis measurements to investigate the influence of the lipid environment and reconstitution method on the photocycle of the receptor alone and in complex with *Np*HtrII$_{157}$. The light-induced transient absorption changes of *Np*SRII-L159R1 and *Np*SRII-L159R1/*Np*HtrII$_{157}$ reconstituted in liposomes, NLPs and SMALPs with the corresponding global multi-exponential fits are shown for three characteristic wavelengths (400, 500 and 550 nm) in Fig. 3. The absorption time traces for *Np*SRII reconstituted in purple membrane lipids (PML) are plotted as a reference. *Np*SRII reconstituted into SMALPs from *E.coli* membranes showed photocycle time traces indistinguishable from those of *Np*SRII treated with DDM and reconstituted into SMALPs from liposomes. Thus, the following analyses are based only on the data of the latter. In the depicted time window shown in Fig. 3, the traces monitored at 500 nm represent the recovery of the *Np*SRII initial state, the traces at 400 nm are indicative for the decay of intermediate M, whereas the formation and decay of the O-state are monitored at 550 nm.

The time constants from the multi-exponential fits are given in Table 1, the corresponding amplitude spectra are shown in Fig. 4. The optical transients with the proteins reconstituted in liposomes and NLPs required three-exponential functions for fitting. The addition of a fourth apparent time constant as fitting parameter did neither increase the quality of the fits nor was its value significant. Contrarily, in the case of SMALPs four-exponential functions were required to describe the optical transients properly, similar to the findings for these proteins reconstituted in purple membranes (30).

The time traces for *Np*SRII-L159R1 and *Np*SRII-L159R1/*Np*HtrII$_{157}$ in liposomes and NLPs do not show significant differences in the recovery of the initial state, and there is no large influence of the NLP environment on the equilibrium between

the M- and O-intermediates (Fig. 3). Minor differences in the time constants are obvious only for τ_8, which appears to be prolonged for the protein complexes reconstituted in NLPs. The decay of intermediate M for both preparations is dominated by time constants τ_7 and τ_8 (cf. Fig. 4 and Table 1). In contrast, in PML the decay of intermediate M is mainly characterized by τ_6 (cf. Ref, 30 and Table 1) and thus approximately three times faster (Fig. 3B). The lifetime of intermediate M strongly depends on the pH of the environment (48), with the reprotonation of the Schiff base being favored by a low pH of the environment. The deceleration of the M-decay in liposomes and NLPs observed in the present experiments may thus be due to the different surface charge densities of the membrane made of *E. coli* lipid extract compared to the purple membrane. The purple membrane consists of two major negatively charged lipid components, phosphatidylglycerophosphate (PG) (70%) and a glycolipid sulfate (20%), which provide the membrane with a large negative surface charge density (49,50). In contrast, bilayers made of *E. coli* polar lipids (~58% neutral phosphatidylethanolamine (PE) and ~15% PG) have a much lower bilayer surface charge density of anionic lipids. The local pH at the lipid/water interface of the present liposomes and NLPs is thus higher than that of the purple membrane (51), which in turn decelerates reprotonation of the Schiff base.

The decay of intermediate M is significantly accelerated for *Np*SRII-L159R1 and *Np*SRII-L159R1/*Np*HtrII$_{157}$ reconstituted in SMALPs, and a transient accumulation of the intermediate O is obvious (Fig. 3B,C). According to the amplitude spectra (Fig. 4), the decay of intermediate M is dominated by τ_5 and τ_6 and is thus one order of magnitude faster than that of the protein preparations in liposomes or NLPs (Table 1). A reasonable explanation for this behavior is the presence of a high local concentration of proton donors provided by the SMA polymer. The pKa values of the two carboxylic groups in each monomol of the 3:1 SMA were found to be well separated with pKa values at ~5.8 and ~8.6. Thus, at pH 8, the presence of the polymer belt increases the negative surface charge density of the SMALPs because one of the acidic groups is always deprotonated, and, in addition, provides a high local concentration of proton donors by the presence of the second carboxylic group with a pKa close to the pH of the bulk. The resulting fast decay of intermediate M in combination with unaltered decay rates of the O-state, τ_7 and τ_8, leads to a larger accumulation of the latter in SMALPs compared to liposomes or NLPs (Fig. 3B,C).

Due to the partial spectral overlap of the *Np*SRII initial state and the O-state (see Fig. 4), the recovery time of the initial state in SMALPs seems to be accelerated by a factor of 6-7 as compared to the proteins in liposomes or NLPs. However, comparison of the time constants τ_7 and τ_8 (Table 1) for NLPs and SMALPs show that the decay of intermediate O and the recovery

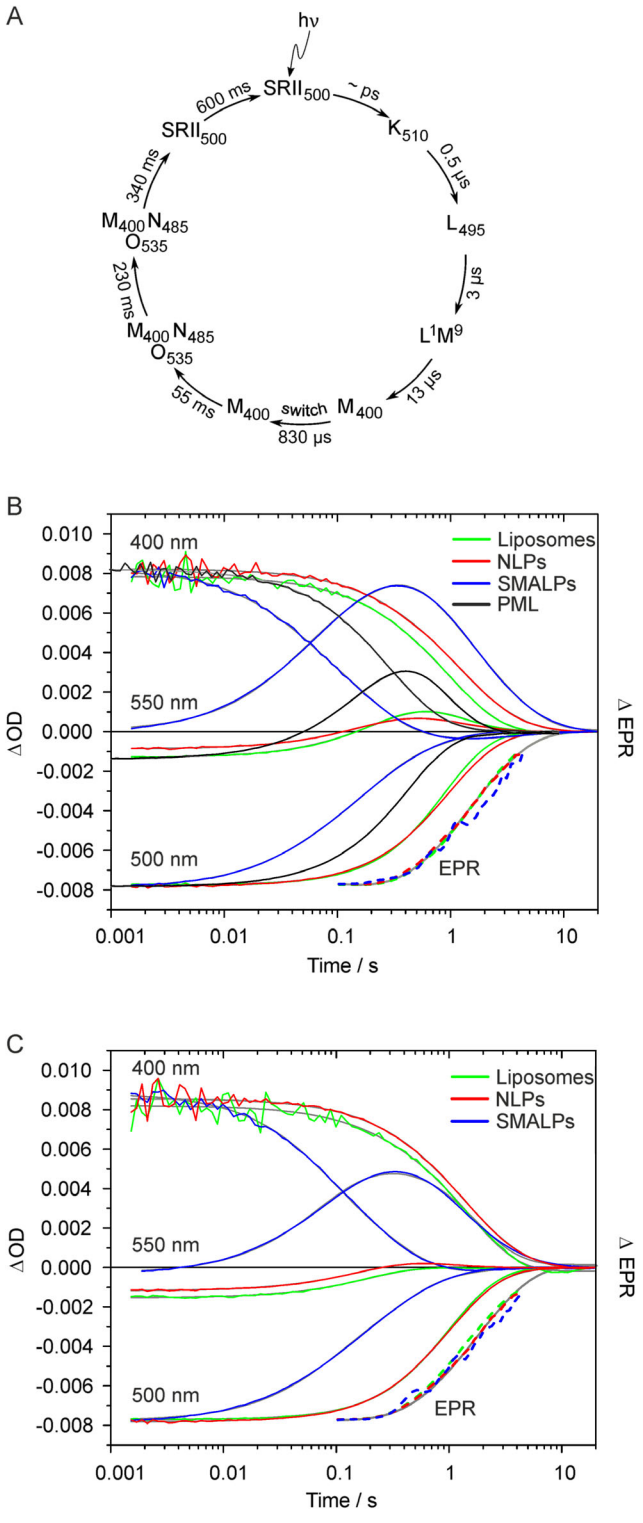

Figure 3. (A) *Np*SRII photocycle determined by following the transient changes in the optical absorption spectrum of the retinal chromophore. Subscript numbers indicate the wavelength of maximum absorption of the intermediate in nm. Time constants characterizing the transitions in the second half of the photocycle are given according to the values and nomenclature of Wegener *et al.* (30) Transient optical absorption changes and transient EPR signals for *Np*SRII-L159R1 in the absence (B) and presence (C) of *Np*HtrII$_{157}$-wt reconstituted in PML (solid black, only shown in B), in liposomes (solid green (optical), dashed green (EPR)), NLPs (solid red (optical), dashed red (EPR)) and SMALPs (solid blue (optical), dashed blue (EPR)). The exponential fits for both optical and EPR transients are depicted in solid gray. Transient optical absorption changes are recorded at 25°C at wavelengths characteristic for the sensory rhodopsin photocycle: 400 nm (M-intermediate), 500 nm (initial state) and 550 nm (O-state). The traces of the M-intermediate, the initial state and the EPR transients are arbitrarily normalized to one of the samples to allow comparison of the kinetics, while the traces of O-intermediate are scaled up using the normalization factors of the corresponding initial state.

Table 1. Time constants determined by exponential fitting for transient optical (Opt.) and EPR spectroscopic data

	PML			Liposomes				NLPs				SMALPs			
				SRII-L159R1		SRII-L159R1/HtrII		SRII-L159R1		SRII-L159R1/HtrII		SRII-L159R1		SRII-L159R1/HtrII	
	SRII Opt.	SRII-L159R1 Opt. (30)	SRII-L159R1/ HtrII Opt. (30)	Opt.	EPR*	Opt.	EPR*	Opt.	EPR*	Opt.	EPR*	Opt.	EPR*	Opt.	EPR*
τ_5/ms	-	55	62	-	-	-	-	-	-	-	-	35 ± 2	-	44 ± 2.8	-
τ_6/ms	237 ± 43	230	240	267 ± 34	154 ± 6 (−30%)	205 ± 57	143 ± 5 (−31%)	182 ± 22	160 ± 24 (−33%)	170 ± 33	170† (−20%)	172 ± 7	172† (−13%)	190 ± 12	190† (−8%)
τ_7/ms	301 ± 58	340	390	660 ± 157	660† (9%)	816 ± 231	816† (33%)	904 ± 84	904† (51%)	934 ± 113	934† (35%)	825 ± 71	825† (20%)	627 ± 54	627† (19%)
τ_8/ms	676 ± 82	600	1300	1170 ± 250	1730 ± 33 (121%)	1500 ± 270	1750 ± 57 (98%)	2450 ± 470	2450† (82%)	2500 ± 500	2300 ± 340 (85%)	2870 ± 140	2870† (93%)	2300 ± 130	2300† (89%)

τ_5-τ_8 represent the results of the four-exponential fittings, and, if τ_5 is not given, τ_6-τ_8 are the results of the three-exponential fittings (numbering of time constants according to Ref. 30). The time constants reported in Ref. 30 for samples reconstituted in PML are given for comparison. *The relative amplitudes of the respective exponentials of the EPR transients are given in parentheses. τ_6 of the EPR transients represents a convolution of the rise time of conformational changes and the rise time of lock-in amplifier, which was set to 100 ms. †The time constants are held fixed according to the values of the optical transients, amplitudes were fitted.

of the initial state follow very similar time courses in both preparations.

Transient conformational changes upon light excitation studied by time-resolved EPR spectroscopy

The effect of the different lipid environments on light-induced conformational changes in *Np*SRII, that is, the outward movement of helix F, is monitored by the transient mobility changes of the nitroxide side chain of *Np*SRII-L159R1 upon light excitation. EPR difference spectra (light–dark) were determined directly during a B-field scan (see Materials and Methods), in the presence and absence of N*p*HtrII$_{157}$, for the protein(s) reconstituted in liposomes, NLPs and SMALPs. Figure 5A–F shows the amplitudes of the transient traces detected at several B-field values (green bars) which build up the light–dark difference spectra. These difference spectra are superimposed onto the dark state cw EPR spectra. Time traces recorded at B-fields with maximum light–dark amplitudes are included in Fig. 3B, C, the time constants of the recoveries are listed in Table 1.

For all lipid environments, considerable light-induced spectral changes could be detected. The amplitudes of the transient spectra in case of liposomes and NLPs were nearly in the same range, whereas for SMALPs the amplitudes of the transient spectra were smaller by a factor of ~ 5. In general, the light–dark difference spectra of L159R1 are not influenced by the presence of the transducer *Np*HtrII$_{157}$ in agreement with earlier work (30). The spectral pattern of the light–dark difference spectra in case of liposomes and NLPs is almost identical (Fig. 5A–D). This type of pattern is in line with an increased nitroxide mobility upon light excitation (see below). In contrast, the light–dark difference spectra for SMALPs (Fig. 5E,F) reveal a different pattern indicating different light-induced conformational nitroxide dynamics and thus suggesting also a different conformational change in the receptor.

In order to characterize the transient light–dark difference spectra in more detail, we used spectral simulations based on the solution of the stochastic Liouville equation (52, 40). The simulated difference spectrum shown in Fig. 5G was obtained by subtracting the simulated spectrum of the dark state (red), characterized by an isotropic reorientational motion of the spin-label side chain with a reorientational correlation time of 16 ns, from a spectrum (black) representing the light-excited state, which is assumed to be characterized by a correlation time of 14 ns. Hyperfine and g-tensor values were fixed. The resulting agreement of the experimental (Fig. 5A–D) with the simulated (Fig. 5G) difference spectra supports our interpretation of a transient increase in the spin-label mobility upon light excitation in liposomes and NLPs. The kinetic properties of the EPR transients are independent from the binding of the transducer fragment in agreement with the results found for the complex in PML (30).

In contrast, the experimental difference spectra for *Np*SRII-L159R1 and *Np*SRII-L159R1/*Np*HtrII in SMALPs (Fig. 5E,F) could not be simulated by a simple light-induced change in the reorientational correlation time of the spin label. In order to achieve reasonable agreement between experiment and simulation, the calculated difference spectrum (Fig. 5H) was determined by subtracting the calculated spectrum of the dark state (red) with a reorientational correlation time of 17 ns and an additional line broadening of 0.78 G from a spectrum (black)

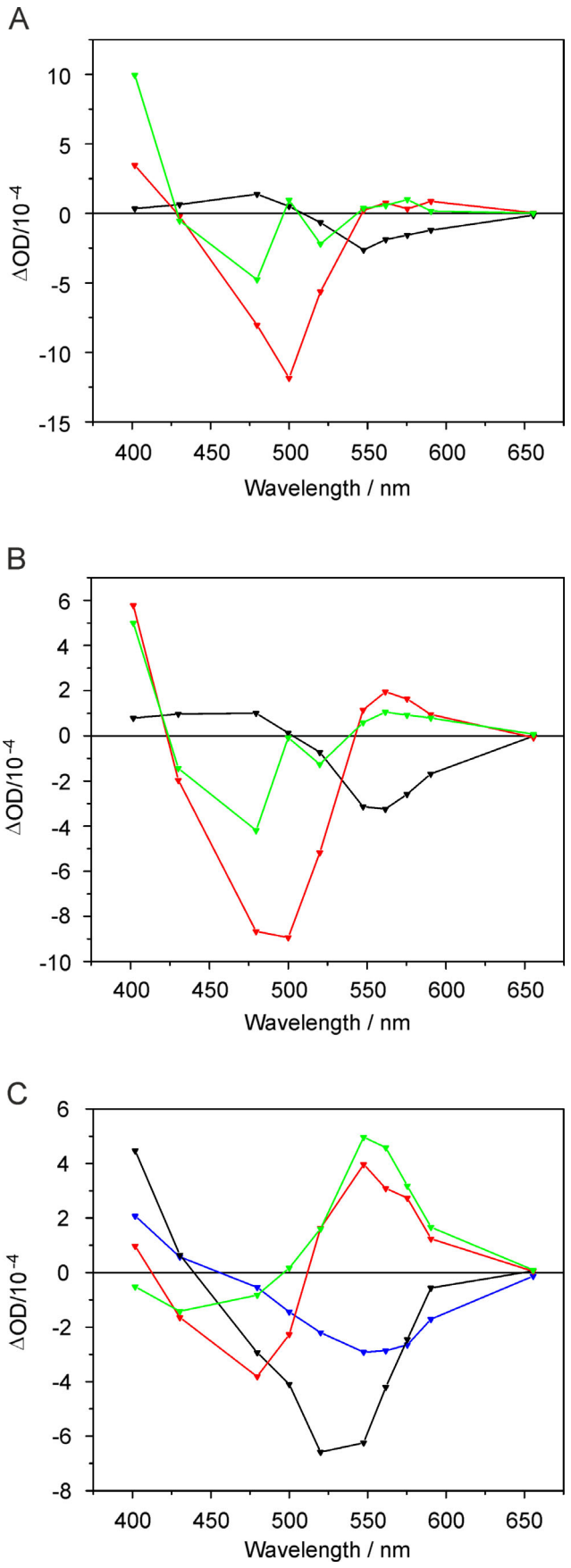

Figure 4. Amplitude spectra corresponding to the exponential time constants, τ_5 (blue), τ_6 (black), τ_7 (red) and τ_8 (green), describing the absorption changes for liposomes (A), NLPs (B) and SMALPs (C). The positive bands at 400 and 550 nm are assigned to the decay of intermediates M and O, respectively. The negative bands at 550 nm represent the rise of the O-state, while at 500 nm they represent the rise of the N-state or of the initial state or a mixture of both, because it is difficult to discriminate between them due to overlapping absorption spectra (the absorption maxima of *Np*SRII initial state and intermediate N are 500 and 485 nm, respectively).

which is characterized by a correlation time of 19 ns and a line broadening of 0.88 G. Consequently, it appears that in case of SMALPs, the spin-label mobility transiently decreases and the line width, which might contain contributions from dipolar spin–spin interaction, increases upon light excitation, the latter indicating that the two L159R1 side chains in the complex come into closer vicinity. Indeed, the interspin distance distribution for the complex in the frozen dark state determined by DEER shows the population maximum of closest approach located at 2.3 nm (25). A light-induced decrease in this distance by movements of helices F toward each other may lead to the observed increase in the line width in the cw EPR spectrum. In conclusion, the conformational changes taking place in *Np*SRII upon light excitation lead to transient dynamics changes in L159R1 which are different in SMALPs compared to the transitions observed in liposomes and NLPs.

In previous studies (30–32), it was shown that the conformational changes observed by the transient increase in the mobility

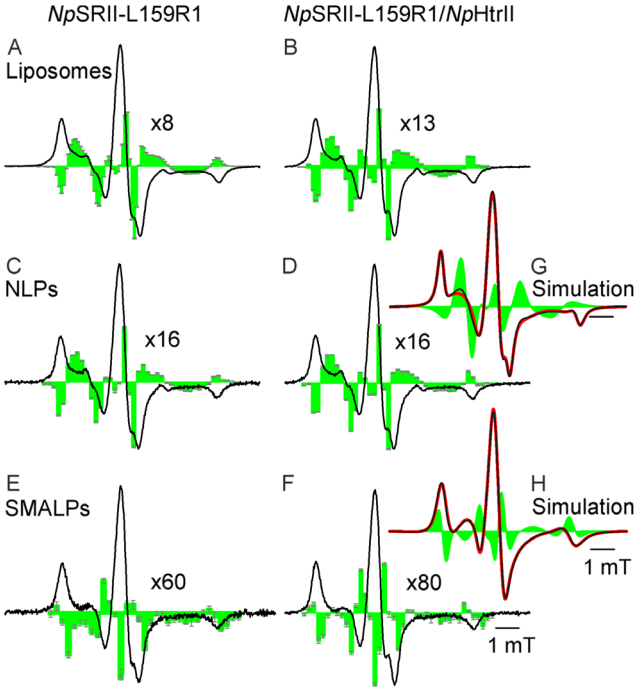

Figure 5. (A–F) Cw EPR spectra (black) and transient EPR light–dark difference spectra (green) obtained after light activation. Scaling factors denote the upscaling of the transient spectra for visibility. (G, H) Spectra were simulated to fit the experimental cw EPR spectra (red), for a slightly increased mobility (G) or for a slightly decreased mobility in combination with an increased line width (H). The calculated difference spectra (green) have been multiplied by a factor of 10 for visibility.

of L159R1 are correlated to the outward tilt of helix F during the long-lived M-intermediate of the *Np*SRII receptor. Disruption of a water cluster connecting helices C and G of *Np*SRII in course of its photocycle permits the necessary conformational freedom of helix F (53). The observed transient mobilization of L159R1 for *Np*SRII in liposomes and NLPs indicates that reconstitution in NLPs does not influence this movement. In contrast, the SMA copolymer and/or lipid environment of SMALPs affect the conformational dynamics of *Np*SRII accompanying the outward tilt of helix F. In liposomes and NLPs, the motional freedom of the nitroxide of L159R1 is transiently increased upon the outward tilt of helix F because sterical interactions between L159R1 and neighboring protein atoms are reduced. For *Np*SRII-L159R1 in SMALPs, the mobility of the nitroxide is transiently more restricted pointing toward a transitional strengthening of its sterical interactions. This may indicate an interaction of the protein with the SMA polymer and/or a reduced flexibility of the lipids in SMALPs compared to NLPs which largely permit conformational changes of the protein that change its shape in the membrane. According to Jamshad *et al.* (27), the styrene moieties of SMA polymer intercalate between the lipid acyl chains perpendicular to the plane of the lipids. In addition, it has been shown that the carboxyl groups of maleic acid interact electrostatically with the head groups of lipids that reside in the outer layer of SMALPs (11,27). Thus, the direct interaction between the SMA polymer and lipids could cause a higher rigidity of the lipid environment, which may hinder conformational changes or helical movement and thus interfere with the protein function (9). Indeed, a motional restriction of bacteriorhodopsin molecules incorporated into SMALPs was already observed (11). In our case of *Np*SRII, similar to the reduced amplitude of the helix F motion observed in crystals of *Np*SRII/*Np*HtrII (53), the conformational freedom of at least the cytoplasmic moiety of helix F is reduced by a more rigid environment in SMALPs.

The decays of the transient EPR signals are compared to the optically detected absorption changes in Fig. 3B,C. To be consistent with the analyses of transient optical data, the EPR transients were fitted using a tri-exponential function. The time constant τ_6 of the EPR transients was necessary to achieve a good fit for all samples. However, we have to be careful to give it a physical meaning because the time constant of the lock-in amplifier of the transient EPR setup was set to 100 ms to achieve decent signal to noise ratios. Thus, the kinetics of EPR transients faster than 100 ms cannot be resolved and the rise time of the EPR signal cannot be properly determined. The values of the decay time constants of the EPR transients, τ_7 and τ_8, prove that the transient EPR signal decay follows the decay of intermediate O for all samples. The formation of the O-state is attributed to the retinal reisomerization from 13-*cis* to *all-trans*, the decay of O includes the rearrangement of the protein conformation to its initial state and coincides with the recovery of the latter. Thus, the transient EPR signal decay mirrors the recovery of the initial position and environment of helix F the time course of which is not affected by the NLP or SMALP environments.

CONCLUSION

The cw EPR data show that reconstitution in NLPs and SMALPs does not affect the spin label side-chain dynamics in the interior of the reconstituted *Np*SRII in its dark state, indicating that the protein's fold close to position 159 is not significantly affected by the lipid environment. At the same time, the cw EPR data of *N*pSRII/*N*pHtrII$_{157}$-A94R1 revealed clear differences in the mobility of the nitroxide close to the membrane-water interface in the SMA-encased *Np*SRII/*Np*HtrII complex compared to NLPs and liposomes. The time-resolved optical spectra show similar kinetics of the photocycle for *Np*SRII reconstituted in liposomes and NLPs. The recovery of the M-state is accelerated in SMALPs due to a high local concentration of protons. Thus, these data confirm that *Np*SRII, reconstituted in SMALPs and NLPs, retains its functionality. The transient EPR light–dark difference spectra revealed light-dependent conformational changes in *Np*SRII and *Np*SRII/*Np*HtrII in liposomes, NLPs as well as in SMALPs. While the transient outward tilt of helix F of *Np*SRII, which has been observed in liposomes during the second half of the photocycle (30), appears to be unaltered in NLPs, in SMALPs this large-scale conformational change seems to be restricted, similar to the reduced amplitude of the helix F motion observed in crystals of *Np*SRII/*Np*HtrII. We conclude that SMALPs could be suitable for the preparation of stable and functional membrane protein samples for spectroscopic investigations of their conformation and dynamics keeping in mind possible restrictions of conformational changes in the transmembrane region of the protein(s).

Acknowledgements—This work was supported by German Research Foundation (DFG, STE640/15) and the Federal Ministry of Education and Research of Germany (BMBF, 05K14MPA).

REFERENCES

1. Nietlispach, D. and A. Gautier (2011) Solution NMR studies of polytopic alpha-helical membrane proteins. *Curr. Opin. Struct. Biol.* **21**, 497–508.
2. Wunnicke, D. and I. Hänelt (2017) The synergetic effects of combining structural biology and EPR spectroscopy on membrane proteins. *Crystals* **7**, 117.
3. Rawson, S., S. Davies, J. D. Lippiat and S. P. Muench (2016) The changing landscape of membrane protein structural biology through developments in electron microscopy. *Mol. Membr. Biol.* **33**, 12–22.
4. Fromme, P. and J. C. Spence (2011) Femtosecond nanocrystallography using X-ray lasers for membrane protein structure determination. *Curr. Opin. Struct. Biol.* **21**, 509–516.
5. Klare, J. P., E. Bordignon, M. Doebber, J. Fitter, J. Kriegsmann, I. Chizhov, H. J. Steinhoff and M. Engelhard (2006) Effects of solubilization on the structure and function of the sensory rhodopsin II/transducer complex. *J. Mol. Biol.* **356**, 1207–1221.
6. Bayburt, T. H. and S. G. Sligar (2010) Membrane protein assembly into nanodiscs. *FEBS Lett.* **584**, 1721–1727.
7. Hernandez-Rocamora, V. M., C. Garcia-Montanes and G. Rivas (2014) Phospholipid bilayer nanodiscs: A powerful tool to study the structural organization and biochemical reactivity of proteins in membrane-like environments. *Curr. Top. Med. Chem.* **14**, 2637–2646.
8. Borch, J. and T. Hamann (2009) The nanodisc: A novel tool for membrane protein studies. *Biol. Chem.* **390**, 805–814.
9. Dorr, J. M., S. Scheidelaar, M. C. Koorengevel, J. J. Dominguez, M. Schafer, C. A. van Walree and J. A. Killian (2016) The styrene-maleic acid copolymer: A versatile tool in membrane research. *Eur. Biophys. J.* **45**, 3–21.
10. Lee, S. C. and N. L. Pollock (2016) Membrane proteins: Is the future disc shaped? *Biochem. Soc. Trans.* **44**, 1011–1018.
11. Orwick-Rydmark, M., J. E. Lovett, A. Graziadei, L. Lindholm, M. R. Hicks and A. Watts (2012) Detergent-free incorporation of a seven-transmembrane receptor protein into nanosized bilayer Lipodisq particles for functional and biophysical studies. *Nano Lett.* **12**, 4687–4692.

12. Ward, R., C. Pliotas, E. Branigan, C. Hacker, A. Rasmussen, G. Hagelueken, I. R. Booth, S. Miller, J. Lucocq, J. H. Naismith and O. Schiemann (2014) Probing the structure of the mechanosensitive channel of small conductance in lipid bilayers with pulsed electron-electron double resonance. *Biophys. J.* **106**, 834–842.
13. Orban-Glass, I., N. Voskoboynikova, K. B. Busch, D. Klose, C. Rickert, W. Mosslehy, F. Roder, V. Wilkens, J. Piehler, M. Engelhard, H. J. Steinhoff and J. P. Klare (2015) Clustering and dynamics of phototransducer signaling domains revealed by site-directed spin labeling electron paramagnetic resonance on SRII/HtrII in membranes and nanodiscs. *Biochemistry* **54**, 349–362.
14. Sahu, I. D., R. M. McCarrick, K. R. Troxel, R. F. Zhang, H. J. Smith, M. M. Dunagan, M. S. Swartz, P. V. Rajan, B. M. Kroncke, C. R. Sanders and G. A. Lorigan (2013) DEER EPR measurements for membrane protein structures via bifunctional spin labels and lipodisq nanoparticles. *Biochemistry* **52**, 6627–6632.
15. Jeschke, G. (2012) DEER distance measurements on proteins. *Annu. Rev. Phys. Chem.* **63**, 419–446.
16. Zou, P. and H. S. McHaourab (2010) Increased sensitivity and extended range of distance measurements in spin-labeled membrane proteins: Q-band double electron-electron resonance and nanoscale bilayers. *Biophys. J.* **98**, L18–L20.
17. McHaourab, H. S., P. R. Steed and K. Kazmier (2011) Toward the fourth dimension of membrane protein structure: Insight into dynamics from spin-labeling EPR spectroscopy. *Structure* **19**, 1549–1561.
18. Dorr, J. M., M. C. Koorengevel, M. Schafer, A. V. Prokofyev, S. Scheidelaar, E. A. van der Cruijsen, T. R. Dafforn, M. Baldus and J. A. Killian (2014) Detergent-free isolation, characterization, and functional reconstitution of a tetrameric K+ channel: The power of native nanodiscs. *Proc. Natl Acad. Sci. USA* **111**, 18607–18612.
19. Morrison, K. A., A. Akram, A. Mathews, Z. A. Khan, J. H. Patel, C. Zhou, D. J. Hardy, C. Moore-Kelly, R. Patel, V. Odiba, T. J. Knowles, M. U. Javed, N. P. Chmel, T. R. Dafforn and A. J. Rothnie (2016) Membrane protein extraction and purification using styrene-maleic acid (SMA) copolymer: Effect of variations in polymer structure. *Biochem. J.* **473**, 4349–4360.
20. Knowles, T. J., R. Finka, C. Smith, Y. P. Lin, T. Dafforn and M. Overduin (2009) Membrane proteins solubilized intact in lipid containing nanoparticles bounded by styrene maleic acid copolymer. *J. Am. Chem. Soc.* **131**, 7484–7485.
21. Gulati, S., M. Jamshad, T. J. Knowles, K. A. Morrison, R. Downing, N. Cant, R. Collins, J. B. Koenderink, R. C. Ford, M. Overduin, I. D. Kerr, T. R. Dafforn and A. J. Rothnie (2014) Detergent-free purification of ABC (ATP-binding-cassette) transporters. *Biochem. J.* **461**, 269–278.
22. Long, A. R., C. C. O'Brien, K. Malhotra, C. T. Schwall, A. D. Albert, A. Watts and N. N. Alder (2013) A detergent-free strategy for the reconstitution of active enzyme complexes from native biological membranes into nanoscale discs. *BMC Biotechnol.* **13**, 41.
23. Swainsbury, D. J. K., S. Scheidelaar, R. van Grondelle, J. A. Killian and M. R. Jones (2014) Bacterial reaction centers purified with styrene maleic acid copolymer retain native membrane functional properties and display enhanced stability. *Angew. Chem. Int. Edit.* **53**, 11803–11807.
24. Paulin, S., M. Jamshad, T. R. Dafforn, J. Garcia-Lara, S. J. Foster, N. F. Galley, D. I. Roper, H. Rosado and P. W. Taylor (2014) Surfactant-free purification of membrane protein complexes from bacteria: Application to the staphylococcal penicillin-binding protein complex PBP2/PBP2a. *Nanotechnology* **25**, 285101.
25. Voskoboynikova, N., W. Mosslehy, A. Colbasevici, T. T. Ismagulova, D. V. Bagrov, A. A. Akovantseva, P. S. Timashev, A. Y. Mulkidjanian, V. N. Bagratashvili, K. V. Shaitan, M. P. Kirpichnikov and H. J. Steinhoff (2017) Characterization of an archaeal photoreceptor/transducer complex from Natronomonas pharaonis assembled within styrene-maleic acid lipid particles. *RSC Adv.* **7**, 51324–51334.
26. Zhang, R., I. D. Sahu, L. Liu, A. Osatuke, R. G. Comer, C. Dabney-Smith and G. A. Lorigan (2015) Characterizing the structure of lipodisq nanoparticles for membrane protein spectroscopic studies. *Biochim. Biophys. Acta* **1848**, 329–333.
27. Jamshad, M., V. Grimard, I. Idini, T. J. Knowles, M. R. Dowle, N. Schofield, P. Sridhar, Y. P. Lin, R. Finka, M. Wheatley, O. R. T. Thomas, R. E. Palmer, M. Overduin, C. Govaerts, J. M. Ruysschaert, K. J. Edler and T. R. Dafforn (2015) Structural analysis of a nanoparticle containing a lipid bilayer used for detergent-free extraction of membrane proteins. *Nano Res.* **8**, 774–789.
28. Royant, A., P. Nollert, K. Edman, R. Neutze, E. M. Landau, E. Pebay-Peyroula and J. Navarro (2001) X-ray structure of sensory rhodopsin II at 2.1-angstrom resolution. *Proc. Natl Acad. Sci. USA* **98**, 10131–10136.
29. Luecke, H., B. Schobert, J. K. Lanyi, E. N. Spudich and J. L. Spudich (2001) Crystal structure of sensory rhodopsin II at 2.4 angstroms: Insights into color tuning and transducer interaction. *Science* **293**, 1499–1503.
30. Wegener, A. A., I. Chizhov, M. Engelhard and H. J. Steinhoff (2000) Time-resolved detection of transient movement of helix F in spin-labelled pharaonis sensory rhodopsin II. *J. Mol. Biol.* **301**, 881–891.
31. Klare, J. P., V. I. Gordeliy, J. Labahn, G. Buldt, H. J. Steinhoff and M. Engelhard (2004) The archaeal sensory rhodopsin II/transducer complex: A model for transmembrane signal transfer. *FEBS Lett.* **564**, 219–224.
32. Klare, J. P., I. Chizhov and M. Engelhard (2008) Microbial rhodopsins: Scaffolds for ion pumps, channels, and sensors. *Results Probl. Cell Differ.* **45**, 73–122.
33. Klare, J. P., E. Bordignon, M. Engelhard and H. J. Steinhoff (2011) Transmembrane signal transduction in archaeal phototaxis: The sensory rhodopsin II-transducer complex studied by electron paramagnetic resonance spectroscopy. *Eur. J. Cell Biol.* **90**, 731–739.
34. Orekhov, P. S., D. Klose, A. Y. Mulkidjanian, K. V. Shaitan, M. Engelhard, J. P. Klare and H. J. Steinhoff (2015) Signaling and adaptation modulate the dynamics of the photosensoric complex of *Natronomonas pharaonis*. *PLoS Comput. Biol.* **11**, e1004561.
35. Shimono, K., M. Iwamoto, M. Sumi and N. Kamo (1997) Functional expression of pharaonis phoborhodopsin in Escherichia coli. *FEBS Lett.* **420**, 54–56.
36. Hohenfeld, I. P., A. A. Wegener and M. Engelhard (1999) Purification of histidine tagged bacteriorhodopsin, pharaonis halorhodopsin and pharaonis sensory rhodopsin II functionally expressed in Escherichia coli. *FEBS Lett.* **442**, 198–202.
37. Mennes, N., J. P. Klare, I. Chizhov, R. Seidel, R. Schlesinger and M. Engelhard (2007) Expression of the halobacterial transducer protein HtrII from Natronomonas pharaonis in *Escherichia coli*. *FEBS Lett.* **581**, 1487–1494.
38. Bayburt, T. H., Y. V. Grinkova and S. G. Sligar (2002) Self-assembly of discoidal phospholipid bilayer nanoparticles with membrane scaffold proteins. *Nano Lett.* **2**, 853–856.
39. Holterhues, J., E. Bordignon, D. Klose, C. Rickert, J. P. Klare, S. Martell, L. Li, M. Engelhard and H. J. Steinhoff (2011) The signal transfer from the receptor NpSRII to the transducer NpHtrII is not hampered by the D75N mutation. *Biophys. J.* **100**, 2275–2282.
40. Klose, D., N. Voskoboynikova, I. Orban-Glass, C. Rickert, M. Engelhard, J. P. Klare and H. J. Steinhoff (2014) Light-induced switching of HAMP domain conformation and dynamics revealed by time-resolved EPR spectroscopy. *FEBS Lett.* **588**, 3970–3976.
41. Wegener, A. A., J. P. Klare, M. Engelhard and H. J. Steinhoff (2001) Structural insights into the early steps of receptor-transducer signal transfer in archaeal phototaxis. *EMBO J.* **20**, 5312–5319.
42. Steinhoff, H. J., R. Mollaaghababa, C. Altenbach, K. Hideg, M. Krebs, H. G. Khorana and W. L. Hubbell (1994) Time-resolved detection of structural-changes during the photocycle of spin-labeled bacteriorhodopsin. *Science* **266**, 105–107.
43. Radzwill, N., K. Gerwert and H. J. Steinhoff (2001) Time-resolved detection of transient movement of helices F and G in doubly spin-labeled bacteriorhodopsin. *Biophys. J.* **80**, 2856–2866.
44. Klare, J. P., E. Bordignon, M. Engelhard and H. J. Steinhoff (2004) Sensory rhodopsin II and bacteriorhodopsin: Light activated helix F movement. *Photochem. Photobiol. Sci.* **3**, 543–547.
45. Doebber, M., E. Bordignon, J. P. Klare, J. Holterhues, S. Martell, N. Mennes, L. Li, M. Engelhard and H. J. Steinhoff (2008) Salt-driven equilibrium between two conformations in the HAMP domain from Natronomonas pharaonis – The language of signal transfer? *J. Biol. Chem.* **283**, 28691–28701.

46. Chizhov, I., G. Schmies, R. Seidel, J. R. Sydor, B. Luttenberg and M. Engelhard (1998) The photophobic receptor from Natronobacterium pharaonis: Temperature and pH dependencies of the photocycle of sensory rhodopsin II. *Biophys. J.* **75**, 999–1009.
47. Schmies, G., B. Luttenberg, I. Chizhov, M. Engelhard, A. Becker and E. Bamberg (2000) Sensory rhodopsin II from the haloalkaliphilic natronobacterium pharaonis: Light-activated proton transfer reactions. *Biophys. J.* **78**, 967–976.
48. Klare, J. P., G. Schmies, I. Chizhov, K. Shimono, N. Kamo and M. Engelhard (2002) Probing the proton channel and the retinal binding site of Natronobacterium pharaonis sensory rhodopsin II. *Biophys. J.* **82**, 2156–2164.
49. Kates, M., S. C. Kushwaha and G. D. Sprott (1982) Lipids of purple membrane from extreme halophiles and of methanogenic bacteria. *Methods Enzymol.* **88**, 98–111.
50. Jonas, R. and T. G. Ebrey (1990) Purple membrane: Surface charge density and the multiple effect of pH and cations. *Photochem. Photobiol.* **52**, 1163–1177.
51. Kundu, A., S. Yamaguchi and T. Tahara (2014) Evaluation of pH at charged lipid/water interfaces by heterodyne-detected electronic sum frequency generation. *J. Phys Chem. Lett.* **5**, 762–766.
52. Budil, D. E., S. Lee, S. Saxena and J. H. Freed (1996) Nonlinear-least-squares analysis of slow-motion EPR spectra in one and two dimensions using a modified Levenberg-Marquardt algorithm. *J. Magn. Reson., Ser. A* **120**, 155–189.
53. Moukhametzianov, R., J. P. Klare, R. Efremov, C. Baeken, A. Goppner, J. Labahn, M. Engelhard, G. Buldt and V. I. Gordeliy (2006) Development of the signal in sensory rhodopsin and its transfer to the cognate transducer. *Nature* **440**, 115–119.